Optical and Quantum Electronics **32:** 211–225, 2000.

Quantum well and quantum dot lasers: From strained-layer and self-organized epitaxy to high-performance devices

PALLAB BHATTACHARYA
Solid State Electronics Laboratory, Department of Electrical Engineering and Computer Science, University of Michigan, Ann Arbor, MI 48109-2122, USA

Abstract. Strained heterostructures are now widely used to realize high-performance lasers. Highly mismatched epitaxy also produces defect-free quantum dots via an island growth mode. The characteristics of high-speed strained quantum well and quantum dot lasers are described. It is seen that substantial improvements in small-signal modulation bandwidth are obtained in both 1 μm (48 GHz) and 1.55 μm (26 GHz) by tunneling electrons directly into the lasing sub-band. In quantum dots the small-signal modulation bandwidth is limited by electron-hole scattering to ~7 GHz at room temperature and 23 GHz at 80 K. The properties of these devices are described.

Key words: electron-hole scattering, hot-carrier effects, performance, quantum dot laser, quantum well laser, tunneling injection

1. Introduction

Lasers with strained quantum well active regions have demonstrated superior performance in terms of gain threshold current, and modulation bandwidth. Even better performance is expected of lasers with quantum dot active regions due to the singular density of states in these low-dimensional quantum confined media. Quantum dots realized by etching have demonstrated limited success in terms of laser performance due to the high density of etch-induced damage. On the other hand, self-organized growth of highly strained semiconductor quantum dots has emerged as a powerful and convenient technique of realizing an ordered array of quantum dots. Room-temperature self-organized quantum dot lasers have also recently been demonstrated (Kamath *et al.* 1996; Mirin *et al.* 1996; Bimberg *et al.* 1996, 1997; Shoji *et al.* 1997). Careful measurements on GaAs-based 1 μm quantum dot lasers indicate that, in spite of the extremely high differential gain ($\sim 10^{-13}$ cm^2) in these devices, the bandwidth is limited to 7 GHz at room temperature. The bandwidth increases to ~20 GHz only at cryogenic temperature.

It is generally believed that spectral hole burning and carrier heating are the two main causes of gain suppression in lasers (Rideout *et al.* 1991; Zhao *et al.* 1992; Girardin *et al.* 1995). Hot carriers are produced as the laser is

pumped harder. They are also produced as the carriers injected into the active region require a finite time (10–40 ps) to thermalize into the lasing sub-band in the quantum wells. The carrier distribution therefore changes from a quasi-Fermi distribution to a hot-carrier distribution, as illustrated in Fig. 1, and a substantive part of the injected carrier density ends up as wasted charge. This eventually leads to higher threshold current, larger Auger recombination, higher-frequency chirp, lower modulation bandwidth and a larger temperature dependence of the threshold current.

At high levels of injection current, the stimulated emission time approaches 10–15 ps. If injected carriers, which are 'cold', can be supplied at this rate, or faster, then the carrier distribution will remain quasi-Fermi, and most of the deleterious effects mentioned above can be minimized or eliminated. This is the basis of the tunneling injection laser. The properties of high-speed 1 and 1.55 μm tunneling injection quantum well and quantum dot lasers will be described in this paper.

2. State-of-the-art GaAs- and InP-based strained quantum well lasers

Strained-layer multiple quantum well (MQW) structures have been used to obtain large modulation bandwidth of semiconductor lasers. The differential gain increases with the number of wells because of the reduced carrier density per well, and the state-filling effect due to carrier population in optical confinement layers is less detrimental for a MQW laser than a single QW laser. The strain in a QW also increases the differential gain, but it also increases the nonlinear gain coefficient making the damping factor relatively unchanged (Ralston *et al.* 1993). The heterostructure band offset in the QW should be large to obtain large differential gain (Zhao *et al.* 1992) and small damping factor, but too large a band offset will result in carrier trapping and injection heating which will lower the

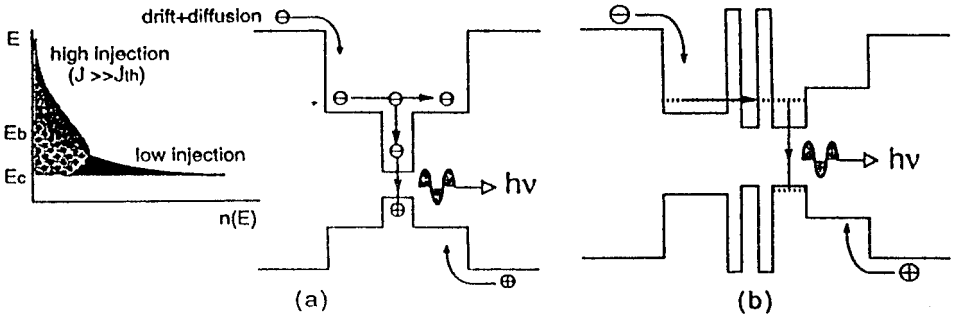

Fig. 1. Band diagrams and carrier injection process in (a) SCH lasers, (b) single-well tunneling injection lasers.

bandwidth (Tsai *et al.* 1995). To enhance the high speed laser performance, the number, strain, and band offset of MQW devices should be optimized together with other parameters such as well size and doping (Uomi *et al.* 1990). In general, the gain and differential gain are higher in GaAs, compared to those in InP or InGaAsP. Furthermore, the electron wells are deeper in the GaAs-based heterostructures. Therefore, it is expected that the intrinsic modulation bandwidths are higher in GaAs-based quantum well lasers, than in InP-based 1.55 μm lasers. This has been borne out by experiments.

The conventional wisdom in achieving large modulation bandwidth is to use graded carrier confining layers and very short cavity lengths (≤100 μm). Hole-modulation doping [Weisser *et al.* 1992] of the active wells further enhances the bandwidth by increasing the differential gain. The largest modulation bandwidth measured in InGaAs/GaAs pseudomorphic QW 1 μm lasers is 40 GHz under CW operation [Weisser *et al.* 1996].

Lasers with high modulation bandwidth in the 1.55 μm wavelength range are important for fiber optic communications. High modulation bandwidths have been measured in 1.55 μm lasers at cryogenic temperatures [Yu *et al.* 1994], and with self-pulsation in distributed Bragg reflector lasers [Schatz *et al.* 1997]. High modulation bandwidths have also been achieved with InGaAlAs barriers and 20 quantum-well structures [Matsui *et al.* 1997], and in p-doped active region buried heterostructure (BH) devices [Morton *et al.* 1992a]. The best measured modulation bandwidth in InP-based 1.55 μm lasers is ~30 GHz.

3. Tunneling injection lasers

Hot carriers give rise to several deleterious effects in lasers. Recently, we have demonstrated the tunneling injection (TI) laser [Bhattacharya *et al.* 1996], in which carrier heating is avoided by tunneling electrons directly into the lasing sub-band. The carrier distribution in the lasing well is governed by the thermalization time of carriers injected by tunneling, rather than by the relaxation time of carriers injected over the barriers, leasing to a 'cold' carrier distribution even at high injection levels. The tunneling times were measured by us [Sung *et al.* 1995] using picosecond time resolved differential transmission spectroscopy (DTS) in a standard pump-probe setup. The 'cold' carrier distribution and the reduction of gain suppression in the TI lasers promise higher modulation bandwidth, lower chirp, and reduced Auger recombination. At the same time, the tunneling barrier prevents electrons from going over the active region into the opposite cladding layer and, therefore, it is expected that the temperature dependence of the threshold current will be reduced. Furthermore, since the initial carrier

distribution injected by tunneling has a smaller energy spread the spectral purity will improve.

Table 1 shows the schematic cross section of a GaAs-based MQW TI laser structure. The device structure consists of a 0.5-μm thick n^+-GaAs buffer, a 1-μm thick n-$A1_{0.6}Ga_{0.4}As$ ($n = 5 \times 10^{17}$ cm^{-3}) outer cladding layer, a 0.1-μm thick undoped GaAs n-side inner cladding or electron injection layer, a 30-Å undoped AlAs tunneling barrier, the active region consisting of four undoped $In_{0.2}Ga_{0.8}As$ QWs with different well widths (64, 54, 50 and 48 Å with 70-Å GaAs barriers in between), a 250-Å thick undoped $A1_{0.1}Ga_{0.9}As$ p-side inner cladding layer a 1-μm thick p-$A1_{0.6}Ga_{0.4}As$ ($p = 5 \times 10^{17}$ cm^{-3}) outer cladding layer and finally a 0.2-μm thick p^+-GaAs (3×10^{19} cm^{-3}) top contact layer. The QW barrier is GaAs in the 4-QW structure and $GaAs_{0.92}P_{0.08}$ in the 6-QW structure to compensate the strain in the active region. The structure was grown on (0 0 1) GaAs substrate by metal-organic vapor phase epitaxy (MOVPE). Fig. 2(a) shows the energy band diagram and the electron wave functions of the MQW TI laser structure under a forward bias, which were obtained by solving the time-independent Schrodinger equation. The wave functions of the first five states are shown. Fig. 2(b)

Table 1. GaAs-based tunneling injection laser heterostructures

0.1 μm	Contact GaAs	p^+ (5×10^{18} cm^{-3})
1.0 μm	Outer clad $Al_{0.60}Ga_{0.40}As$	p (5×10^{17} cm^{-3})
0.1 μm	Inner clad $Al_{0.30}Ga_{0.70}As$	i
80 Å	Active well $In_{0.10}Ga_{0.90}As$	i
20 Å	Resonant tunneling barrier AlAs	i
40 Å	Tunneling well $In_{0.10}Ga_{0.90}As$	i
20 Å	Tunneling barrier AlAs	i
0.1 μm	Inner clad GaAs	i
1.0 μm	Outer Clad $Al_{0.60}Ga_{0.40}As$	n (5×10^{17} cm^{-3})
0.7 μm	Contact GaAs, S. I. GaAs (1 0 0) Substrate	n^+ (5×10^{18} cm^{-3})

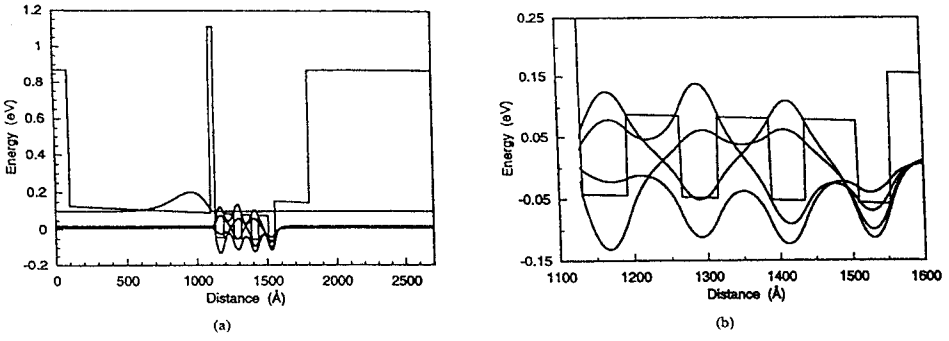

Fig. 2. (a) Conduction band diagram and electron wave functions of MQW tunneling injection lasers and (b) expanded view of the wave functions.

shows an expanded view of the wave functions in the quantum-well regions. It can be seen that the wave functions of the first four states are localized in the four QWs and the wave function of the fifth state, which is the ground state in the cladding layer, is localized in the injection layer (inner cladding layer on the *n*-side). The widths of the QWs and the thickness of the GaAs barrier are optimized so that each of the four wave functions in the QWs is not localized in an individual well but distributed in the MQWs and the energies of these four states are very close to each other. The coupling of the QWs is important for obtaining a uniform carrier distribution in the MQW structure.

Fig. 3 shows the light versus current (*L–I*) characteristics of the MQW TI laser with 4 QWs. The threshold current is 3 mA for a cavity length of 200 μm. The slope efficiency is 0.33 mW/mA and the differential quantum efficiency is 0.52. The peak of the laser emission is at about 0.98 μm, which confirms lasing from the $In_{0.2}Ga_{0.8}As$-GaAs MQW region. The characteristic temperature T_o is 178 K, which was obtained in the temperature range between 20–80°C. Fig. 4(a) shows the modulation frequency response of undoped MQW TI lasers under CW operation. The maximum modulation bandwidth was obtained at 70 mA. The measurement was made up to 40 GHz, which is limited by the amplifier and the spectrum analyzer used in the setup and the modulation response at 40 GHz is about 0 dB. The resonance frequency f_r at 70 mA is 23.5 GHz. The −3-dB modulation bandwidth obtained by the curve fitting is 43 GHz. Under pulsed bias condition, the resonance frequency is 26 GHz and the modulation response at 40 GHz is about 6 dB, shown in Fig. 4(b). The extrapolated −3-dB modulation band-

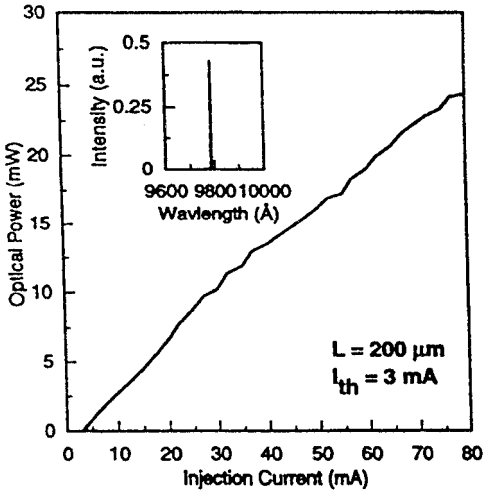

Fig. 3. Light versus current (*L–I*) characteristics of MQW tunneling injection lasers. The inset shows the output spectrum.

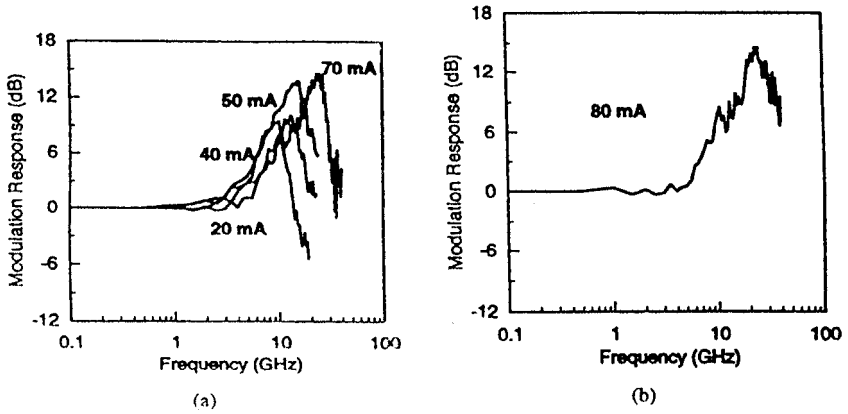

Fig. 4. (a) Modulation frequency response of undoped MQW tunneling injection lasers under CW and (b) pulsed bias conditions.

width is 48 GHz. This is the highest modulation bandwidth reported to date for any semiconductor laser.

The measured frequency response of the laser was fitted to the standard small-signal modulation response to extract modulation parameters, such as the resonance frequency f_r and the damping rate γ as a function of the bias current (Morton *et al.* 1992b; Tatham *et al.* 1992). The resonance frequency is proportional to square root of the output power. From the slope of the linear dependence shown in Fig. 5(a) we obtained the value of the figure of merit $D = 5.06\ \text{GH}/(\text{mW})^{\frac{1}{2}}$ and the differential gain $\mathrm{d}g/\mathrm{d}n = 1.86 \times 10^{-15}\ \text{cm}^2$. The damping rate γ varies linearly with f_r squared, and the proportionality constant is the K-factor (Tatham *et al.* 1992): $K = 4\pi^2[\tau_{ph} + \varepsilon/(v_g \mathrm{d}g/\mathrm{d}n)]$, where τ_{ph} is the photon life time, ε is the gain compression

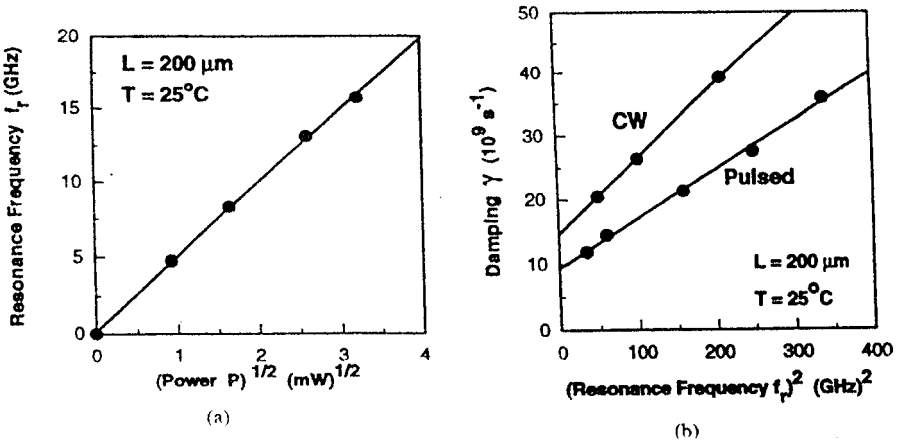

Fig. 5. (a) Plot of f_r versus $P^{\frac{1}{2}}$; (b) damping γ versus f_r^2 of undoped MQW tunneling injection lasers.

coefficient, v_g is the group velocity of light, and dg/dn is the differential gain. The maximum possible intrinsic modulation bandwidth is determined solely by the K-factor, $f_{-3dB\ max} = 2^{3/2}\pi/K$. From a plot of the damping rate against the resonance frequency squared, shown in Fig. 5(b), the K-factor was obtained to be 0.116 ns under CW bias condition, representing a maximum intrinsic bandwidth of 76 GHz. Under pulsed bias K is 0.090 ns and $f_{-3dB\ max} = 98$ GHz. These are the highest maximum intrinsic modulation bandwidth reported to date for semiconductor lasers. From the values of K-factor and differential gain the gain compression coefficient ε is calculated to be 1.5×10^{-17} cm^3 for pulsed bias and 1.7×10^{-17} cm^3 for CW operation. The gain compression is minimized in TI lasers.

Fig. 6 shows the measured variation of threshold current and slope efficiency with temperature in a 0.98 μm MQW-TI laser. Unlike other lasers, a distinct temperature independent region ($T_o > 600$ K) is obtained for $T \leq 60$ K. This confirms that the thermal width of the electron distribution in these is quite narrow and hence the carrier distribution is cold, as expected. The slope efficiency also shows a 'flat' region at low temperature and the typical 'humped' behavior at higher temperatures.

The measured frequency-dependent electrical impedance of an MQW TIL at various drive currents is shown in Fig. 7. From analysis of these data, the carrier capture time is obtained as 1 ps at 50 mA, which agrees with the tunneling time measured directly by differential transmission spectroscopy. Recent simulations by Grupen and Hess (1997), using the Minilase-II simulator have clearly shown that in the TI laser, the electrons tunneling into the QW have low initial energies and therefore, minimizes carrier and phonon heating.

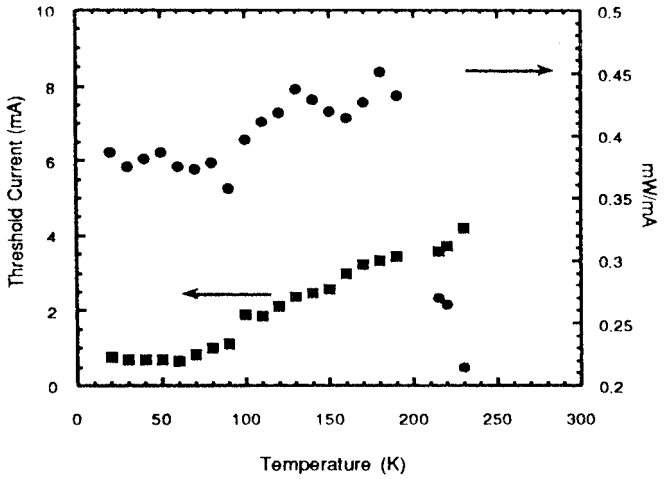

Fig. 6. Temperature dependence of threshold current and slope efficiency in InGaAs 1 μm TIL laser.

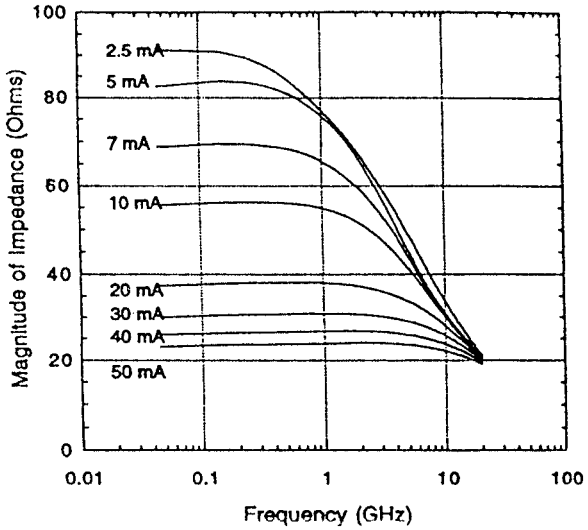

Fig. 7. Magnitude of measured electrical impedance of undoped tunneling injection lasers at various bias currents.

We have also fabricated and characterized InP-based 1.55 μm TI lasers. We have investigated both Fabry–Perot (FP) and distributed feedback (DFB) devices. A typical heterostructure of the FP device is shown in Fig. 8. The measured light–current characteristics are shown in Fig. 9. From these

0.1 μm	In0.53Ga0.47As	p+(1×10^{19} cm^{-3})
0.05 μm	In0.53Ga0.47As graded to InP	p+(1×10^{19} cm^{-3})
1 μm	InP	p+(1×10^{19} cm^{-3})
0.2 μm	InP	p+(1×10^{19} cm^{-3})
0.05 μm	In0.8Ga0.2As0.43P0.57	undoped
8 ×		
0.007 μm	In0.48Ga0.52As0.83P0.17, 0.9% tensile strain	undoped
0.008 μm	In0.70Ga0.24As0.83P0.17, 1% compressive strain	undoped
0.003 μm	InP	undoped
0.1 μm	In0.7Ga0.3As0.63P0.37	undoped
0.2 μm	InP	n(2×10^{17} cm^{-3})
1 μm	InP	n(2×10^{18} cm^{-3})
0.05 μm	InP graded to In0.53Ga0.47As	n(2×10^{18} cm^{-3})
0.5 μm	In0.53Ga0.47As	n+(1×10^{19} cm^{-3})
	SI InP substrate	

Fig. 8. Layer heterostructure of TIL InP laser.

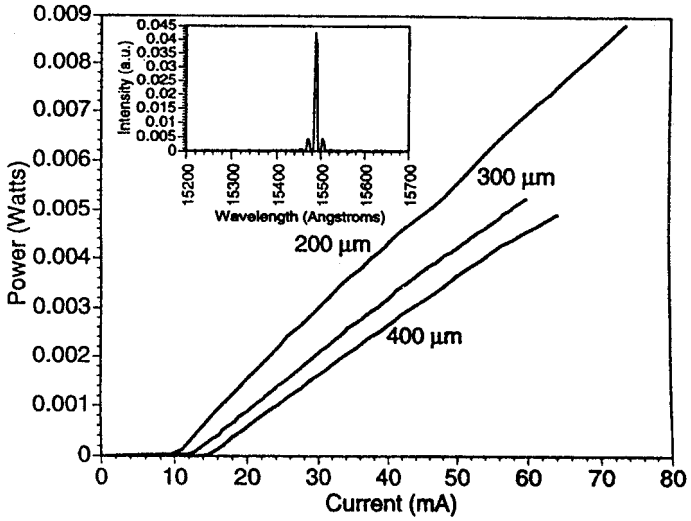

Fig. 9. Light versus current curves for lasers of various lengths. The inset shows the spectrum of a 200 μm device at 25 mA.

curves a value of η_i of 0.61 and internal loss α of 40 cm^{-1} are calculated. The inset shows the spectrum for a 200 μm device at 25 mA.

The optical modulation frequency response of the devices were measured by two separate test facilities and the characteristics are depicted in Figs. 10(a) and (b). The measured bandwidths ranged from 14–20 GHz under CW bias conditions. From these characteristics the maximum differential gain is obtained to be 1×10^{-15} cm^2 and the lowest value of the gain compression factor ε is 5×10^{-17} cm^3. To our knowledge, this is the highest measured bandwidth recorded for an InP-based simple ridge waveguide structure. The carrier escape time τ_{esc} is determined to be 0.5 ns, independent of bias. This high frequency performance is achieved with a very simple device structure at room temperature under constant drive currents.

1.55 μm DFB lasers were made with the same active TI region shown in Fig. 8, incorporating the grating with electron-beam writing and subsequent regrowth to complete the device structure. The temperature-dependent *L–I* characteristics and threshold current density of these devices are shown in Figs. 11(a) and (b). A value of T_o as high as 120 K is extrapolated from the data at room temperature. The high value of T_o is predominantly attributed to the TI design incorporated in the active region.

4. Self organized quantum dot lasers

The quantum dot lasers were grown by MBE on (0 0 1) GaAs substrates. Self-organized $In_{0.4}Ga_{0.6}As$ dots were formed in the Stranski–Krastanow

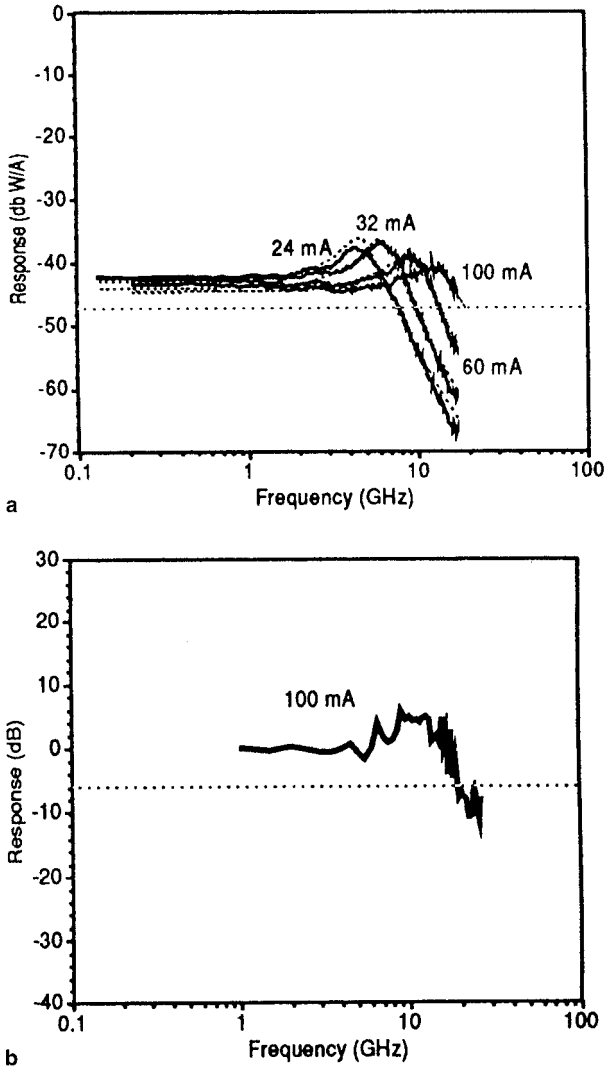

Fig. 10. (a) Bandwidth of 1.55 μm TIL laser measured with Lightwave Test Set. (b) Bandwidth of 1.55 μm TIL laser measured with sweep oscillator/spectrum analyzer.

growth mode. The dots were grown at a substrate temperature of 540°C at a growth rate of ~0.25 monolayer (ML) per second. The 7–9 monolayer deposited consists of a 5–7 ML wetting layer and 2 ML of quantum dots. Subsequent layers of stacked dots require fewer ML deposited before the transition to a 3D RHEED pattern. The rest of the laser is a conventional separate confinement heterostructure laser, with a 0.1 μm GaAs undoped inner cladding and a 1 μm $Al_{0.3}Ga_{0.7}As$ doped outer cladding layer on each side.

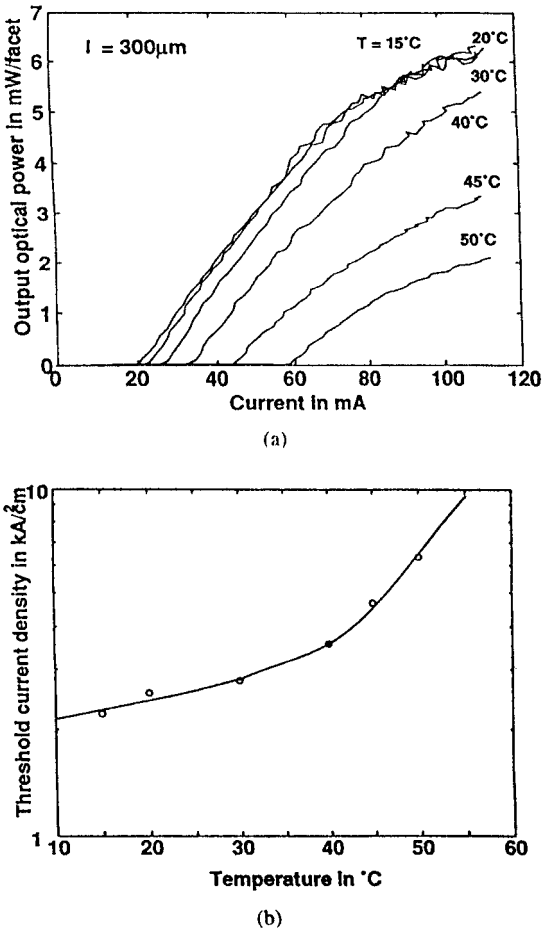

Fig. 11. (a) Temperature dependent L–I characteristics, and (b) J_{th} versus T for 1.55 μm TI-DFB laser.

Single-mode ridge waveguide lasers were made by standard photolithographic techniques. Temperature-dependent light–current and small signal modulation characteristics were measured by mounting the lasers on a heat sink and placing them in a cryogenic chamber with provision for DC and high frequency biasing and for optical output. The optical frequency response was measured as a function of temperature using a photoreceiver, amplifier and network analyzer. The measured threshold current density decreased from 650 A/cm^2 at 300 K to 50 A/cm^2 at 85 K with $T_o = 670$ K in the temperature range $20 \leq T \leq 85$ K (Fig. 12). The very large value of T_o confirms lasing from atomic-like discrete states. The measured modulation bandwidth increases from 5 GHz at 300 K to 23 GHz at 80 K (Fig. 13), which is the highest modulation bandwidth measured in a quantum dot laser. The trend in modulation bandwidth as a function of temperature is com-

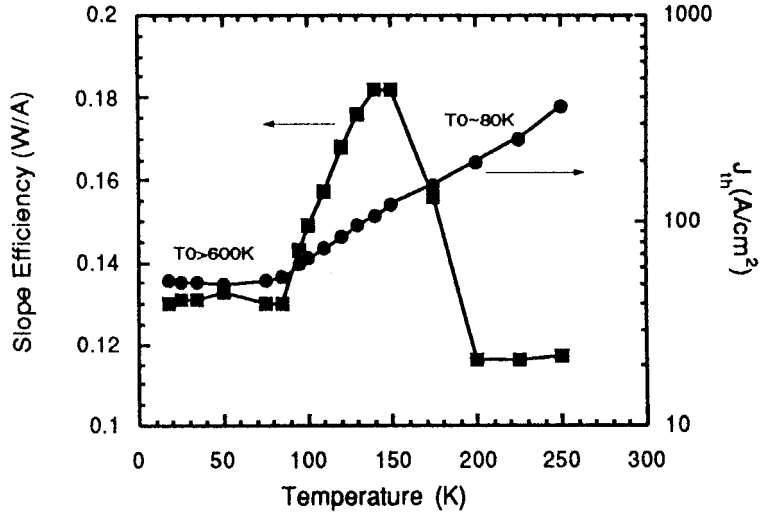

Fig. 12. Threshold current density and slope efficiency for SLQD broad area device.

plemented by earlier measurements of electron capture time of ~30 ps at 300 K and 8 ps at 4 K from laser high-frequency small-signal impedance data (Klotzkin *et al.* 1997) and pump-probe differential transmission spectroscopy (Sosnowski *et al.* 1998), respectively. These dynamic characteristics indicate that the likely mechanism for carrier capture in quantum dots is electron-hole scattering. Calculated values of capture times due to electron-hole scattering are 75 ps at 300 K and 30 ps at 77 K, which are similar in magnitude and trend to the measured data. The differential gain increases from 5×10^{-14} cm^2 at 300 K to $\sim 10^{-13}$ cm^2 at cryogenic temperatures.

From analysis of sets of modulation data at each temperature, the *K*-factor (which determines the damping limit) was extracted as a function of temperature (Fig. 14). Assuming $K = 4\pi^2(\tau_{cap}\eta_{eq}^2 + \tau_p)$ (where τ_p is photon lifetime and η_{eq} is a measure of dot carrier density) the hole quasi-Fermi level is at the ground hole state, and the capture time $\tau_{cap} \sim f_v(E_1 - E_2)$ (i.e., the capture time depends on the number of vacancies), allows us to extract the energy separation $E_1 - E_2$ between the ground and excited electron states. The value of $(E_1 - E_2) = 60$ meV determined in this way is in excellent agreement with the theoretically calculated value of 56 meV and the observed separation between photoluminescent peaks of 70–80 meV. This is quantitative corroborative evidence that the mechanism for carrier capture in quantum dots is electron-hole scattering. It also models how changing the temperature, or engineering the separation between excited and ground energy state, can change the carrier capture time to suit the application.

It is evident that the carrier capture bottleneck presented by electron-hole scattering can possibly be overcome by tunneling electrons directly into the lasing sub-band. The design of such a laser is, however, far more difficult

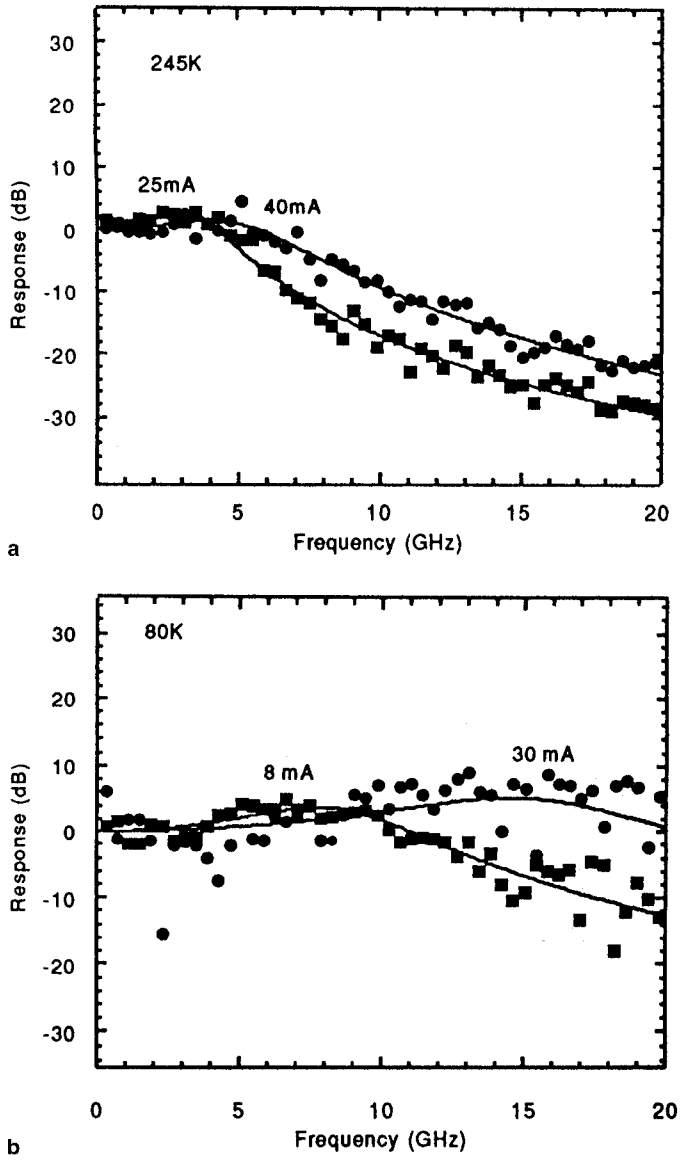

Fig. 13. (a) Measured bandwidth of MLQD laser at 245 K, with bandwidth of 7 GHz. (b) Measured bandwidth of MLQD laser at 80 K, with bandwidth of 23 GHz.

than that for a quantum well TI laser. First, in a quantum dot laser, lasing occurs from the ground states or excited states depending on the number of dot layers and the level of injection. Second, the bandstructure engineering of the tunneling process is slightly complicated by the ~15% dot size non-uniformity. However, we are investigating such a device structure and some improvement in room temperature bandwidths are expected.

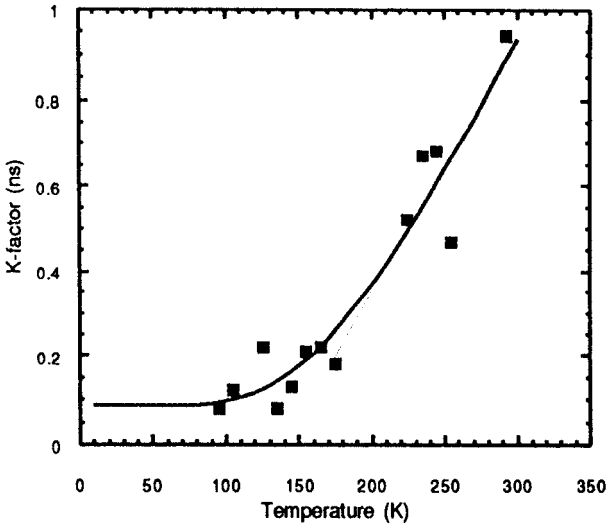

Fig. 14. Measured and fit *K*-factor vs. temperature in MLQD laser.

5. Conclusion

Properties of high-speed strained quantum well and quantum dot lasers are described. TI of electrons substantially enhances the high speed performance of quantum well lasers due to a suppression of hot-carrier effects. The modulation bandwidth of quantum dot lasers are limited by electron-hole scattering. It is apparent that quantum dot lasers will become important devices for future applications.

Acknowledgements

The author acknowledges the contributions by his colleagues and graduate students, past and present. The work is supported by ARO, NSF, DARPA, and ONR.

References

Bhattacharya, P., J. Singh, H. Yoon, X. Zhang, A. Gutierrez-Aitken and Y. Lam. 'Tunneling injection lasers: A new class of lasers with reduced hot carrier effects'. *IEEE J. Quantum Electron.* **32** 1620, 1996.

Bimberg, D., N.N. Ledenstov, O. Stier, D. Bimberg, V.M. Ustinov, P.S. Kop'ev and Zh.I. Alferov. 'InAs-GaAs quantum pyramid lasers: *In situ* growth, radiative lifetimes and polarization properties'. *Jpn. J. Appl. Phys.* **35** 1311, 1996.

Bimberg, D., N. Kirstaedter, N.N. Ledenstov, Zh.I. Alferov, P.S. Kop'ev and V.M. Ustinov. 'InGaAs-GaAs quantum dot lasers'. *IEEE J. Select. Topics in Quantum Electron.* **3** 196, 1997.

Girardin, F., G. Duan, P. Gallion, A. Talneau and A. Qugazzaden. 'Experimental investigation of the relative importance of carrier heating and spectral-hole-burning on nonlinear gain in bulk and strained multi-quantum-well 1.55 μm lasers'. *Appl. Phys. Lett.* **67** 771, 1995.

Grupen M. and K. Hess. 'Severe gain suppression due to dynamic carrier heating in quantum well lasers'. *Appl. Phys. Lett.* **70** 808, 1997.

Kamath, K., P. Bhattacharya, T. Sosnowski, T. Norris and J. Philips. 'Room temperature operation of $In_{0.4}Ga_{0.6}As/GaAs$ self-organized quantum dot lasers'. *Electron. Lett.* **32** 1374, 1996.

Klotzkin, D., K-C. Syao, P. Bhattacharya, C. Caneau and R. Bhat. 'Modulation characteristics of high speed ($f_{-3dB} = 20$ GHz) tunneling injection InP/InGaAsP 1.55 μm ridge waveguide lasers extracted from optical and electrical measurements'. *J. Lightwave Technol.* **15** 2141, 1997.

Matsui, Y., H. Murai, S. Arahira, S. Kutsuzawa and Y. Ogawa. '30 GHz bandwidth 1.55 μm strain-compensated InGaAlAs-InGaAsP MQW laser'. *IEEE Photon. Tech. Lett.* **9** 25, 1997.

Mirin, R., A. Gossard and J. Bowers. 'Room temperature lasing from InGaAs quantum dots'. *Electron. Lett.* **32** 1732, 1996.

Morton, P.A., R.A. Logan, T. Tanbun-Ek, P.F. Sciortino, Jr., A.M. Sergent, R.K. Montgomery and B.T. Lee. '25 GHz bandwidth 1.55 μm GaInAsP *p*-doped strained multiquantum-well lasers'. *Electron. Lett.* **28** 2156, 1992.

Morton, P.A., T. Tanbun-Ek, R.A. Logan, A.M. Sergent, P.F. Sciortino, Jr. and D.L. Coblentz. 'Frequency response subtraction for simple measurement of intrinsic laser dynamic properties'. *IEEE Photon. Tech. Lett.* **4** 133, 1992b.

Ralston, J.D., S. Weisser, I. Esquivias, E.C. Larkins, J. Rosenzweig, P.J. Tasker and J. Fleissner. 'Control of differential gain, nonlinear gain, and damping factor for high-speed application of GaAs-based MQW lasers'. *IEEE J. Quantum Electron.* **29** 1648, 1993.

Rideout, W., W.F. Sharfin, E.S. Koteles, M.O. Bassell and B. Elman. 'Well-barrier hole burning in quantum well lasers'. *IEEE Photon. Tech. Lett.* **3** 784, 1991.

Schatz, R., O. Kjebon, S. Lourdudoss, S. Nilsson and B. Stalnacke. '30 GHz direct modulation bandwidth in detuned loaded InGaAsP DBR lasers at 1.55 μm wavelength'. *Electron. Lett.* **33** 488, 1997.

Shoji, H., Y. Nakara, K. Mukai, Y. Sugiyama, M. Sugawara, N. Yokoyama and H. Ishikawa. 'Temperature dependent lasing characteristics of multi-stacked quantum dot lasers'. *Appl. Phys. Lett.* **71** 193, 1997.

Sosnowski, T.S., T.B. Norris, H. Jiang, J. Singh, K. Kamath and P. Bhattacharya. 'Rapid carrier relaxation in $In_{0.4}Ga_{0.6}As/GaAs$ quantum dots characterized by differential transmission spectroscopy'. *Phys. Rev.* **B57** R9423, 1998.

Sung, C.Y., T.B. Norris, X. Zhang, Y.L. Lam, I. Vurgaftman, J. Singh and P. Bhattacharya. 'Studies of carrier relaxation in low dimensional structures', presented at the Modulated Semiconductor Structures Conference, Spain, July 1995.

Tatham, M.C., I.F. Lealman, Colin P. Seltzer, L.D. Westbrook and D.M. Cooper. 'Resonance frequency, damping, and differential gain in 1.5 μm multiple quantum-well lasers'. *IEEE J. Quantum Electron.* **28** 408, 1992.

Tsai, C.-Yi, C.-Yao Tsai, Y.-H. Lo, R.M. Spencer and L.F. Eastman. 'Nonlinear gain coefficients in semiconductor quantum-well lasers: effects of carrier diffusion, capture, and escape'. *J. Select. Topics Quantum Electron.* **1** 316, 1995.

Uomi, K., T. Mishima and N. Chinone. 'Modulation-doped multi-quantum well (MD-MQW) lasers. I. Experiment'. *Jpn. J. Appl. Phys.* **29** 88, 1990.

Weisser, S., J.D. Ralston, E.C. Larkins, I. Esquivias, P.J. Tasker, J. Fleissner and J. Rosenzweig. 'Efficient high-speed direct modulation in *p*-doped $In_{0.35}Ga_{0.65}As/GaAs$ multiquantum well lasers'. *Electron. Lett.* **28** 2141, 1992.

Weisser, S., *et al.* 'Damping-limited modulation bandwidths up to 40 GHz in undoped short-cavity $In_{0.35}Ga_{0.65}As$-GaAs multiple-quantum-well lasers'. *IEEE Photon. Tech. Lett.* **8** 608, 1996.

Yu, R., R. Nagarajan, T. Reynolds, A. Homes, J. Bowers, S. DenBaars and C. Zah. 'Ultrahigh speed performance of a quantum well laser at cryogenic temperatures'. *Appl. Phys. Lett.* **65** 528, 1994.

Zhao, B., T.R. Chen and A. Yariv. 'The extra differential gain enhancement in multiple-quantum-well lasers'. *IEEE Photon. Tech. Lett.* **4** 124, 1992.